The influence of precursor selection on electrochemical properties of RF thermal plasma synthesized graphene

Maciej Fronczak[1*], Zoltán Károly[2], Predrag Banković[3], Zorica Mojović[3*]

[1]*Department of Molecular Engineering, Faculty of Process and Environmental Engineering, Lodz University of Technology, Wólczańska 213, 93-005 Łódź, Poland*

[2]*Institute of Materials and Environmental Chemistry, Research Centre for Natural Sciences, Magyar tudósok körútja 2, 1117 Budapest, Hungary*

[3]*University of Belgrade, Institute of Chemistry, Technology and Metallurgy, Department for Catalysis and Chemical Engineering - National Institute of the Republic of Serbia, Njegoševa 12 11000 Belgrade, Serbia*

*Corresponding authors:

Maciej Fronczak: *maciej.fronczak@p.lodz.pl*

Zorica Mojović: *zorica.mojovic@ihtm.bg.ac.rs*

Abstract

Electrochemical characterization of a series of graphene samples synthesized by radiofrequency thermal plasma jet is reported. Six simple organic compounds including alkanes, carboxylic acids, alcohols and aldehydes were applied as precursors for graphene synthesis. The Electrochemical characterization was performed by cyclic voltammetry (CV) The response of the selected sample toward 3-nitrophenol and 4-nitrophenol was investigated in the pH range from 2 to 9. The electroanalytical performance of the selected sample for simultaneous detection of these nitrophenols was tested by square wave voltammetry (SWV). The aim of this work was to establish the influence of graphene precursor on its electrochemical properties. The highest current response was obtained from a graphene sample prepared from methane. The simultaneous detection of two nitrophenol derivatives was successful in a concentration range from 10 μM to 500 μM using as-synthesized methane-originated graphene.

Keywords:

Graphene, Radiofrequency thermal plasma, Electrode kinetics, Nitrophenol, Electrochemical sensor

1. Introduction

Carbon-based electrodes have various industrial applications, from metallurgy to battery production. The properties such as high conductivity, good mechanical and thermal properties, availability, and chemical stability [1,2] enabled a wide range of applications. Diverse carbon electrodes such as graphite, glassy carbon, highly oriented pyrolytic graphite and diamond electrodes have been used [3,4]. The need to enhance the properties of these electrodes led to the investigation of nanosized carbon-based materials: carbon nanotubes, fullerenes, carbon quantum dots, nano-diamond and graphene and graphene derivatives [5].

Among carbon-based materials, special attention was devoted to the investigation of graphene and its derivatives. Since the groundbreaking work by Geim and Novoselov [6], which is usually considered as a start of graphene investigation, graphene has been the topic of much research and is a promising candidate for various applications. One of the key applications of graphene in electrochemistry is its utilization as an electrode material. Graphene-based electrodes have shown remarkable performance in various electrochemical processes, such as energy storage [7], electrocatalysis [8], and sensing [9].

The electrochemical activity of graphene is affected by various properties of the graphene such as defects, type and amount of functional groups and the presence of impurities [10]. Two major structural regions of graphene are the basal plane (sp^2 bonded carbon atoms in the form of honeycomb) and the edge plane (perpendicular to basal plane, one carbon atom width plane ending in various functional groups). Pristine (perfect) graphene, i.e. high quality graphene, with a low amount of defects, and low oxygen content shows slow electron transfer kinetics [11]. The presence of this kind of graphene on the electrode surface blocks the electrode's activity. It was established that graphene electroactivity mainly originates from the edge sites, while the electroactivity of the basal plane is negligible [12,13]. Lai et al. [14] established that the freshly prepared basal plane can exhibit electrochemical activity, but this activity decreased with time. The activity of the basal plane can be increased by introduction of defects [15,16].

On the other hand, the expressed electroactivity of graphene also depends on the analyte. Compton et al. showed that the adsorption of guanine at the basal plane, prior to its oxidation on the edge sites significantly affects the height of the current response [17].

The other factor affecting the electroactivity of graphene is the amount and the type of oxygen species at its surface. The literature data report both positive [18] and negative impacts [19] of these groups of the activity of graphene-based electrodes on their electroanalysis performance

for specific analytes. The desirable oxygen species can be obtained by oxidation of graphene [20] or by (electro)reduction of graphene oxide [21].

The properties of graphene vary depending on the method of preparation employed. The synthesis technique used to produce graphene can influence its structural, electrical, mechanical, and chemical properties. The methods are usually divided into bottom-up and top-down approaches [22]. The most commonly used methods are mechanical exfoliation (scotch tape method), chemical exfoliation, chemical vapor deposition (CVD), epitaxial growth and plasma methods. Each graphene synthesis method has its advantages and limitations, and the choice of method depends on the desired application and scalability requirements. The advantage of the thermal plasma decomposition method is that it can be performed under continuous conditions and without a catalyst, which significantly reduces the cost of graphene production [23].

The aim of this investigation was to determine the electrochemical properties of graphene synthesized by RF thermal plasma using different precursor compounds. The electrochemical activity of the graphene material obtained in this manner was tested by two common redox probes. The activity toward nitrophenols enabled the assessment of the activity of samples for both oxidation (of the phenol group) and reduction (of the nitro group). In the end, the electroanalytical performance of a selected sample of unaltered, as-produced graphene for simultaneous detection of 3-nitrophenol (3-NP) and 4-nitrophenol (4-NP) was tested. In order to enhance graphene electroanalytical performance, graphene is usually functionalized [24,25]. Sometimes, the purpose and the effect of functionalization are not easily elucidated [26]. Therefore, the results presented in this paper might be of significance for selecting graphene synthesis parameters in regard to the analyte and prior to possible functionalization.

2. Experimental

2.1 Materials

The graphene samples were obtained via RF plasma jet method described in detail in Supplementary Data and previous works [23,27]. Basing on the physicochemical characterization, already shown in previous works [23,27] and Supplementary Data, the graphene samples exhibits nanoflake morphology (Figure S1) and consists of more than 94.7 atomic % of carbon. The remaining percentage is taken by oxygen. Carbon exists in sp^2 hybridization, characteristic for 2D carbon materials.

The compounds applied in the studies: paraffin oil, potassium chloride, potassium hexacyanoferrate(II) trihydrate, potassium hexacyanoferrate(III), hexaaminеruthenium(III) chloride, and Britton–Robinson buffer constituents (H_3PO_4, CH_3COOH and H_3BO_3) were purchased in Merck.

2.2 Electrochemical measurements

Graphene pastes electrode (GPE) was prepared by hand mixing graphene samples obtained from different precursors with the appropriate amount of paraffin oil. The hollow Teflon tube (2 mm diameter) filled with paste to the length of 1 cm served as the working electrode. GPE obtained in this manner was named according to the precursor used to obtain the given graphene sample. The reference electrode was Ag/AgCl in 3 M KCl, while a platinum rod served as a counter electrode. The Autolab electrochemical workstation (Autolab PGSTAT302N, Metrohm-Autolab BV, Netherlands) was used for electrochemical measurements.

The investigation of GPE response toward two redox probes, 1mM $[Ru(NH_3)_6]^{3+/2+}$ and 1 mM $[Fe(CN)_6]^{3-/4-}$ in 0.2 M KCl, was investigated by cyclic voltammetry (CV). CVs were recorded at different scan rates in the range 20 -300 mV s^{-1}. The diffusion coefficient of 7.2×10^{-6} cm^2s^{-1} and 6.5×10^{-6} cm^2s^{-1} for hexacyanoferrate(II)ion and hexaaminеruthenium(III)ion, respectively, was determined by chronoamperometric measurement [28]. The response of GPE toward 4-NP and 3-NP was performed at various pH values using cyclic voltammetry. The Britton–Robinson buffer (0.1 M H_3PO_4, 0.1 M CH_3COOH and 0.1 M H_3BO_3) was titrated with 1 M NaOH to adjust pH to be in the range of 2 – 9.

The determination of 4-NP and 3-NP was performed by square wave voltammetry from equimolar solutions in Britton-Robinson buffer at pH 5. The optimized conditions used for recording curves for the calibration plot were: deposition potential -1.2 V; deposition time 30 s; pulse amplitude 0.06 V, step 0.005 V and frequency 25 Hz.

3. Results and Discussion

The first examination of different graphene paste electrodes was performed by cyclic voltammetry using two redox probes, $[Fe(CN)_6]^{3-/4-}$ and $[Ru(NH_3)_6]^{3+/2+}$.

Cyclic voltammograms recorded for all electrodes in 1 mM $[Fe(CN)_6]^{3-/4-}$ in 0.2 M KCl are presented in Figures 1a and b. Recorded CVs are grouped into two figures according to the electrode's performance for clarity.

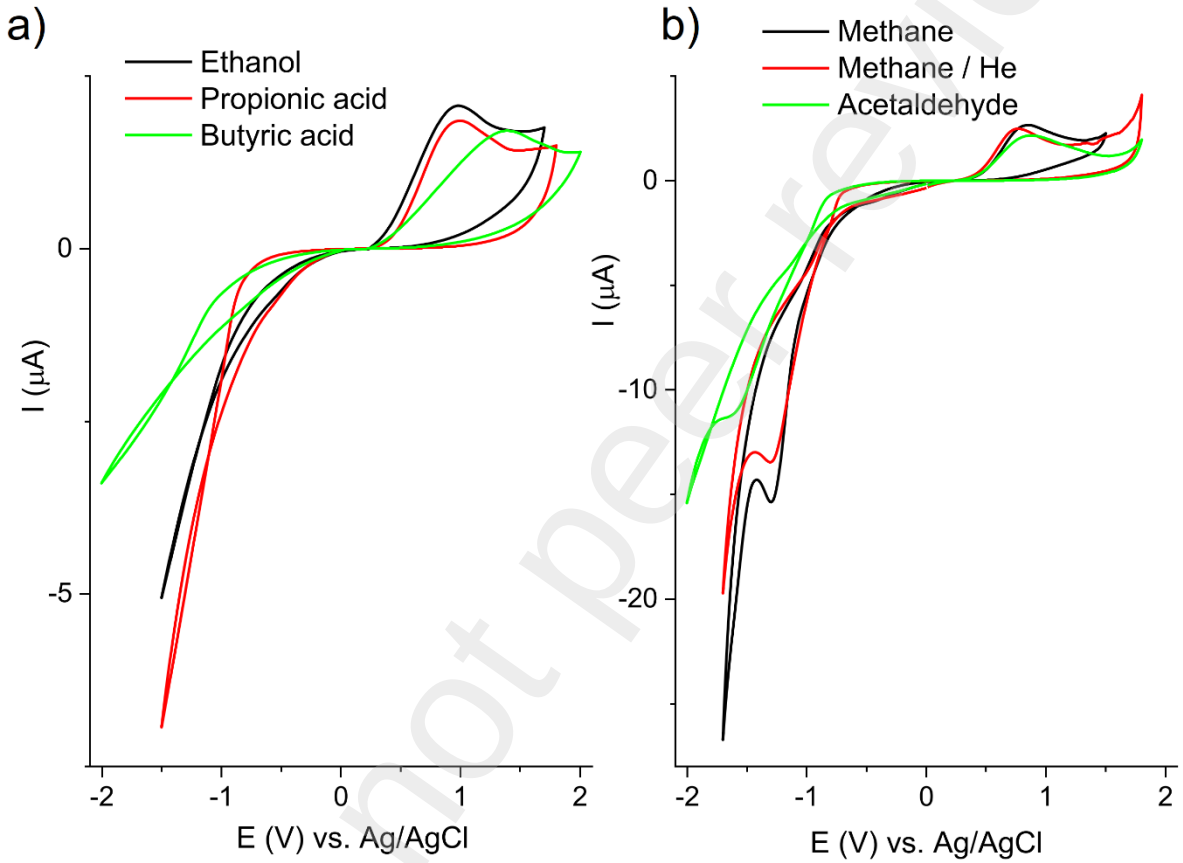

Figure 1: Cyclic voltammograms recorded in 1 mM $[Fe(CN)_6]^{3-/4-}$ + 0.2 M KCl at the scan rate of 50 mV s^{-1}.

The CV of electrodes presented in Figure 1a exhibited only an anodic peak, while a cathodic peak was absent. The CV of electrodes presented in Figure 1b exhibited a pair of peaks, but with very high peak-to-peak separation. This behavior is indicative of very slow kinetics of charge transfer. The investigation of the scan rate has an influence on voltammetric characteristics (Figures S3 – S8) showed linear dependence of peak height on the square root of scan rate, indicating that the electrochemical process was diffusion controlled. The electrochemical heterogeneous standard rate constant (k^0) can be determined from the shift of peak potential with scan rate by the equation [29]:

$$E_{pa} = E^{0'} + \frac{RT}{(1-\alpha)nF}\left[0.78 + \ln\frac{\sqrt{D_R}}{k^0} + \ln\sqrt{\frac{(1-\alpha)nFv}{RT}}\right] \quad (1)$$

where R, T and F are the universal gas constant, absolute temperature and Faraday constant, respectively, D_R is the diffusion coefficient of the reduced species, k^0 is the heterogeneous standard rate constant, α is the energy transfer coefficient and n is the number of electrons transferred during the heterogeneous reaction. The values of the standard electrochemical rate constant are presented in Table 1.

Table 1. The values of the standard electrochemical rate constant

electrode	$[Fe(CN)_6]^{3-/4-}$ k^0 (cm s^{-1})	$[Ru(NH_3)_6]^{2+/3+}$ k^0 (cm s^{-1})
Ethanol	2.7×10^{-5}	1.4×10^{-4}
Propionic acid	4.9×10^{-5}	1.7×10^{-4}
Butyric acid	5.0×10^{-6}	1.1×10^{-5}
Methane	3.5×10^{-3}	2.0×10^{-3}
Methane/He	2.7×10^{-3}	1.4×10^{-3}
Acetaldehyde	1.7×10^{-3}	3.2×10^{-4}

Cyclic voltammograms recorded for all electrodes in 1 mM $[Ru(NH_3)_6]^{2+/3+}$ in 0.2 M KCl are presented in Figures 2a and b. Recorded CVs are grouped by the electrode's performance for clarity. Voltammograms exhibited the expected pair of redox peaks, except for the Butyric acid electrode.

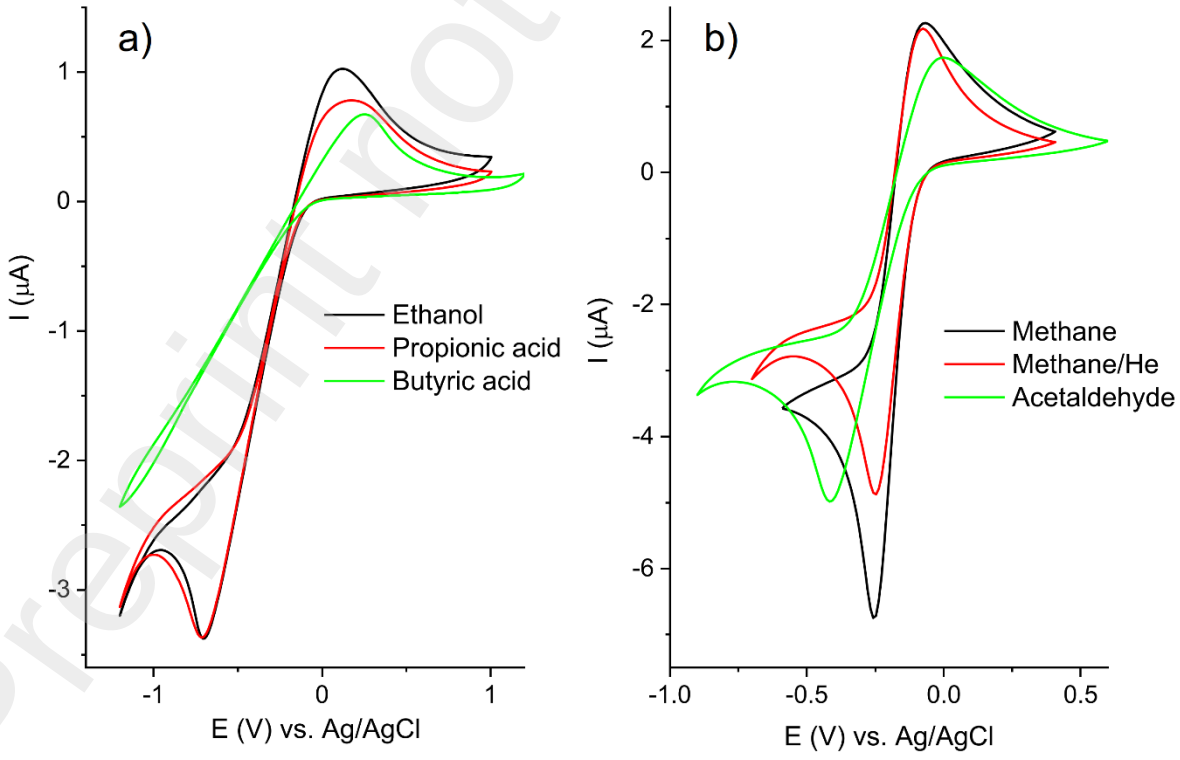

Figure 2: Cyclic voltammograms recorded in 1 mM $[Ru(NH_3)_6]^{2+/3+}$ + 0.2 M KCl at the scan rate of 50 mV s^{-1}.

The highest currents and the lowest value of peak-to-peak separation were obtained for graphene originating from Methane and Methane/He electrodes, indicating that the reversibility of the redox process of $[Ru(NH_3)_6]^{2+/3+}$ probe was highest for these electrodes. However, all obtained values were higher than 59 mV, the expected value for the reversible process. The redox process recorded at the investigated electrode showed to be a quasi-reversible process.

Cyclic voltammograms recorded at different scan rates in the range of 20 – 300 mV s^{-1} are presented in Figures S9 - S14. The peak current showed linear dependence of peak height on the square root of the scan rate, which is characteristic of a diffusion-controlled process. The electrochemical heterogeneous standard rate constant was determined by Lavagnini's modification of the Nicholson method. According to Nicholson's procedure [30], k^0 can be determined as a slope of plot Ψ vs. πDnvF/RT according to the equation:

$$\Psi = k^0[\pi DnvF/RT]^{-1/2} \qquad (2)$$

Nicholson's procedure is applicable for peak-to-peak (ΔE_p) separation values up to 200 mV. The work of Lavagnini et al. [31] modified the procedure to enable its application for higher values of peak-to-peak separation (nxΔEp > 200 mV) according to the equation:

$$\Psi = (-0.6288 + 0.0021X)/(1 - 0.017X) \qquad (3)$$

where X is peak-to-peak separation in mV.

The k^0 value for oxidation of $[Ru(NH_3)_6]^{2+}$ was determined according to the equation (3) for all electrodes except for the Butyric acid electrode. Since the Butyric acid electrode showed irreversible behavior equation (1) was used for the determination of k^0. The obtained values of the heterogeneous rate constant are presented in Table 1.

The values of k^0 for both probes are in accordance with literature data for graphene paste electrodes [32]. The Methane electrode showed the fastest charge transfer kinetics for both probes, while the Butyric acid electrode showed the slowest. It should be noted that values of k^0 obtained for both redox probes should not be considered as absolute values, but only as apparent and indicative rate constants only.

It is considered that $[Ru(NH_3)_6]^{3+/2+}$ probe is not surface sensitive and the response of the electrode toward this probe is determined only by the density electronic states near the formal

potential of the redox system [3,12]. On the other hand, the response of the electrode toward $[Fe(CN)_6]^{4-/3-}$ probe depends, in addition to the electronic structure, on the presence of the oxygenated species on the electrode surface as well [33]. It is considered that the fast charge transfer rate occurs at graphene edges, while the charge transfer is rather slow on basal planes due to their hydrophobic nature [34]. Slow charge transfer kinetics for Ethanol, Propionic acid and Butyric acid electrodes was a consequence of the low amount of edge sites and the presence of carbon-oxygenated species. In this regard, the Acetaldehyde electrode showed an unexpectedly high rate of charge transfer for $[Fe(CN)_6]^{4-/3-}$ probe, considering that the precursor contains oxygen.

In order to better understand the effect of oxygen on the values of the obtained apparent charge transfer rate constant we correlated their values with the values of various oxygen species obtained by XPS measurements (described in previous works [23,27] and shown in Supplementary Data, Figure S2). Both redox species showed similar behavior in correlation with total oxygen (Figure 3). There was a plateau at values 4.3-4.7 atomic % of surface composition.

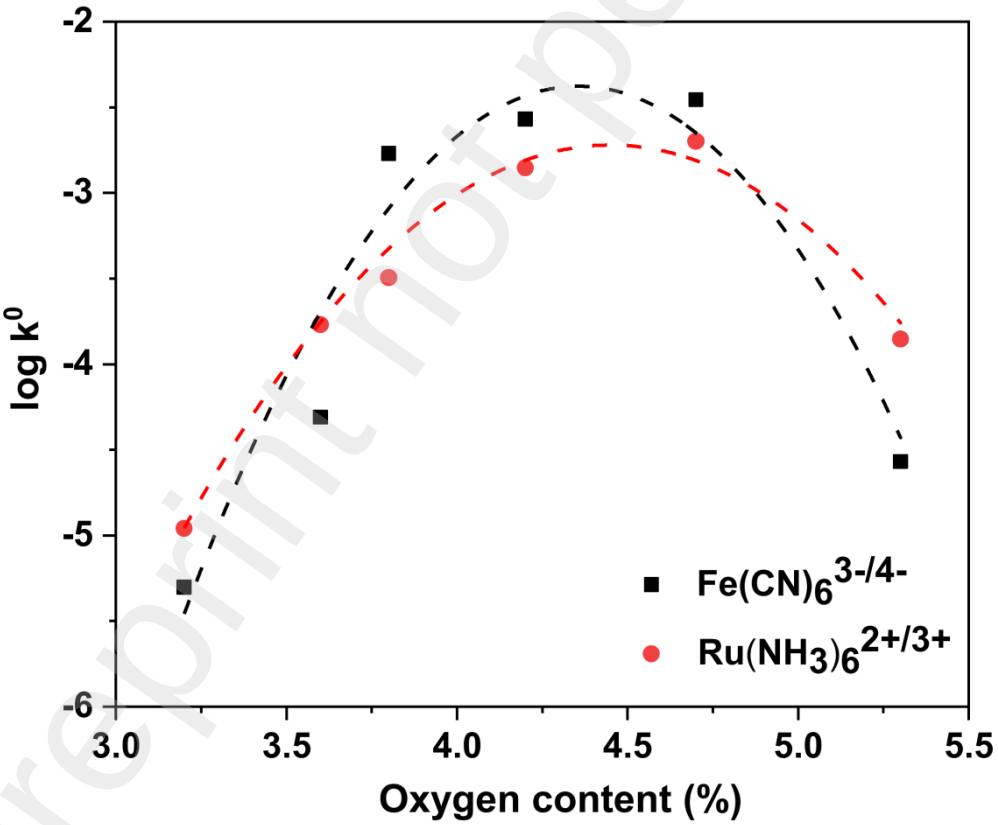

Figure 3. Relation between the decimal logarithm of k^0 and the oxygen surface content determined with XPS.

However, when correlated with lines corresponding to the chemical states it was found that oxygen assigned to C–O–C in ester and OH in the carboxyl, has the most negative effect on the values of apparent charge transfer rate constant for both redox probes. the high amount of C-OH also had a negative effect, while the presence of C=O and C-O-C had a positive effect on the charge transfer kinetics for both redox probes. It follows that the hydroxyl moieties plausibly worsens the charge transfer, whilst the other carbon-oxygen bonds supports the electrochemical reaction onto the surface. These relations are shown in Supplementary Data (Figure S15).

3.5 Electrochemical oxidation of 4-Nitrophenol and 3-Nitrophenol

Further studies were performed with the electrode that showed the highest activity: Methane, Methane/He and Acetaldehyde electrode. The electrochemical behavior of graphene paste electrodes was studied in the presence of 4-nitrophenol and 3-nitrophenol. The nitrophenols contain two functional groups: the -OH group and the NO_2 group. The response of selected electrodes was studied for oxidation and reduction of nitrophenols. The oxidation of nitrophenols was investigated at different pHs, in the range of 2-9. Cyclic voltammograms recorded at the Methane electrode in buffer solution without nitrophenol are presented in Figure 4. Cyclic voltammograms recorded for Methane/He and Acetaldehyde electrodes under the same conditions are presented in Figures S16 and S17.

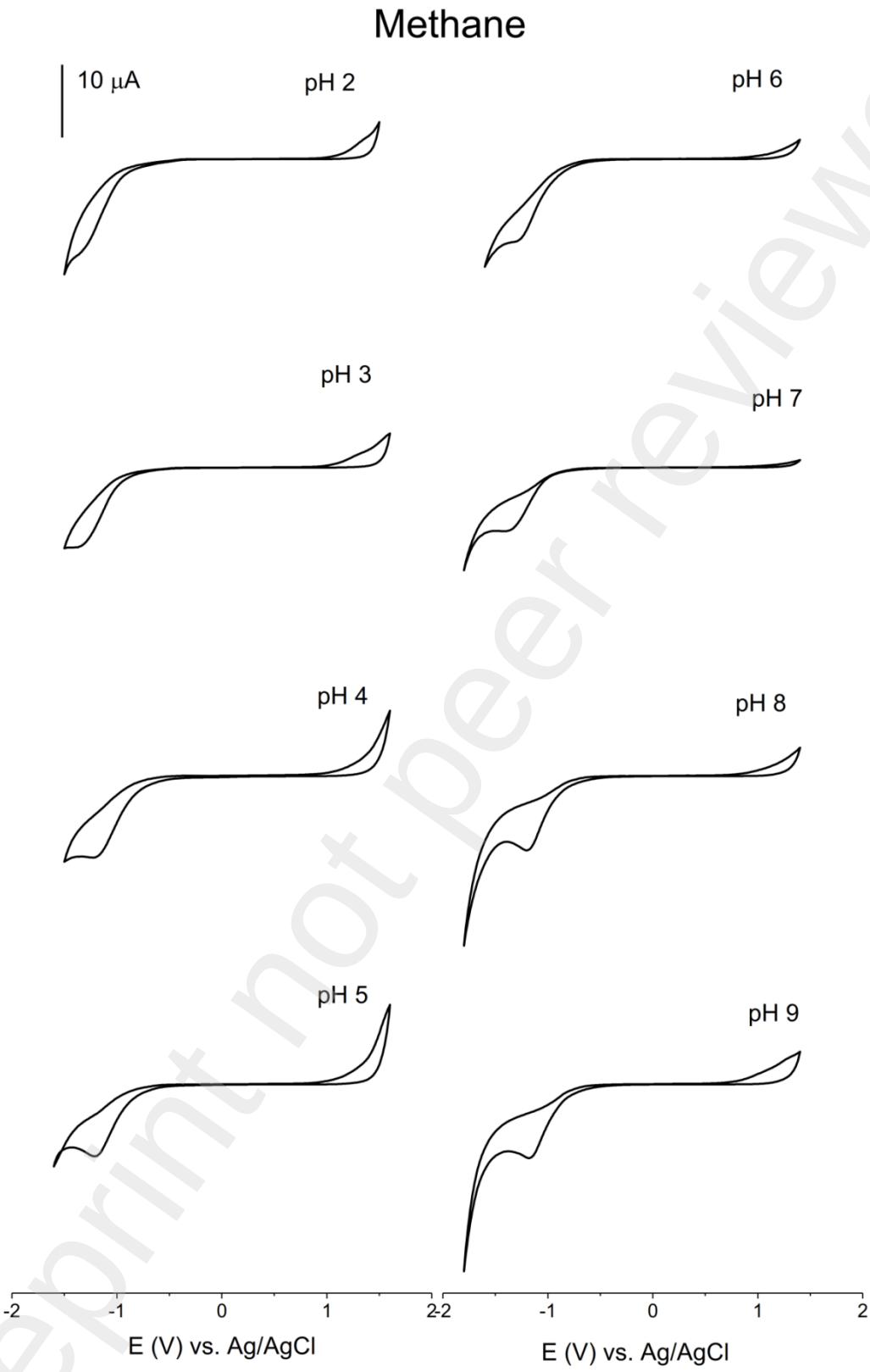

Figure 4: Cyclic voltammograms recorded on Methane electrode in the Britton-Robinson buffer at pH range 2 – 9 at the scan rate of 100 mV s^{-1}

The presence of some oxygen-containing functionalities on the surface of graphene-based materials can be found by cyclic voltammetry. Cyclic voltammograms of Methane, Methane/He and Acetaldehyde electrodes were recorded in Britton-Robinson buffer in the pH range 2-9. The cathodic peak at potential around -1.2 V was visible at all CV recorded at the Methane electrode and Methane/He. CV recorded at the Acetaldehyde electrodes showed the cathodic peak at a more negative potential value, except for pH 2, when only current due to hydrogen evolution was noticeable. According to the literature [35], electrochemically reducible oxygen-containing functionalities are the peroxy (at -0.7 V), aldehyde (at -1.0 V), epoxy (at -1.5 V) and carbonyl (at -2.0 V). Shifting toward negative potential might indicate a higher amount of carbonyl group. Other researchers [36] suggested that negative polarization down to -1.5 V involves a reduction of epoxy and carbonyl groups.

At the foot of the current rise due to the oxygen evolution process, the anodic wave can be seen at the marginal pH value used. This process might be ascribed to the oxidation of the phenol group.

Cyclic voltammograms recorded in the presence of 4-NP and 3-NP for the Methane electrode are presented in Figures 5a and b.

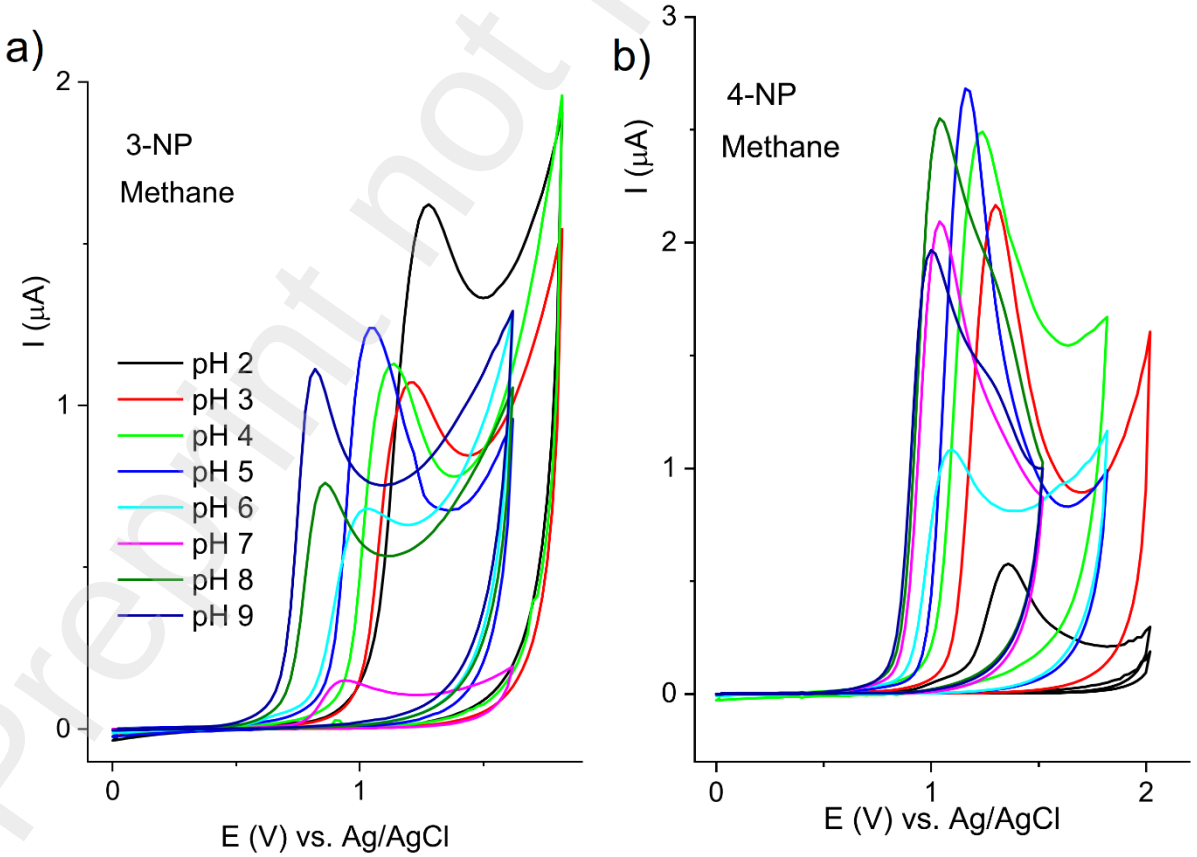

Figure 5: Cyclic voltammograms recorded at Methane electrode at scan rate 100 mV s^{-1} in pH range of 2 -9 for oxidation of a) 3-NP and b) 4-NP. The concentration of nitrophenol was 1mM.

The cyclic voltammograms recorded for Methane/He and Acetaldehyde are given in Supplementary data in Figures S18 and S19.

The dependence of peak potential and peak current for oxidation of 3-NP and 4-NP on pH value is presented in Figures 6 a-d, for all investigated electrodes.

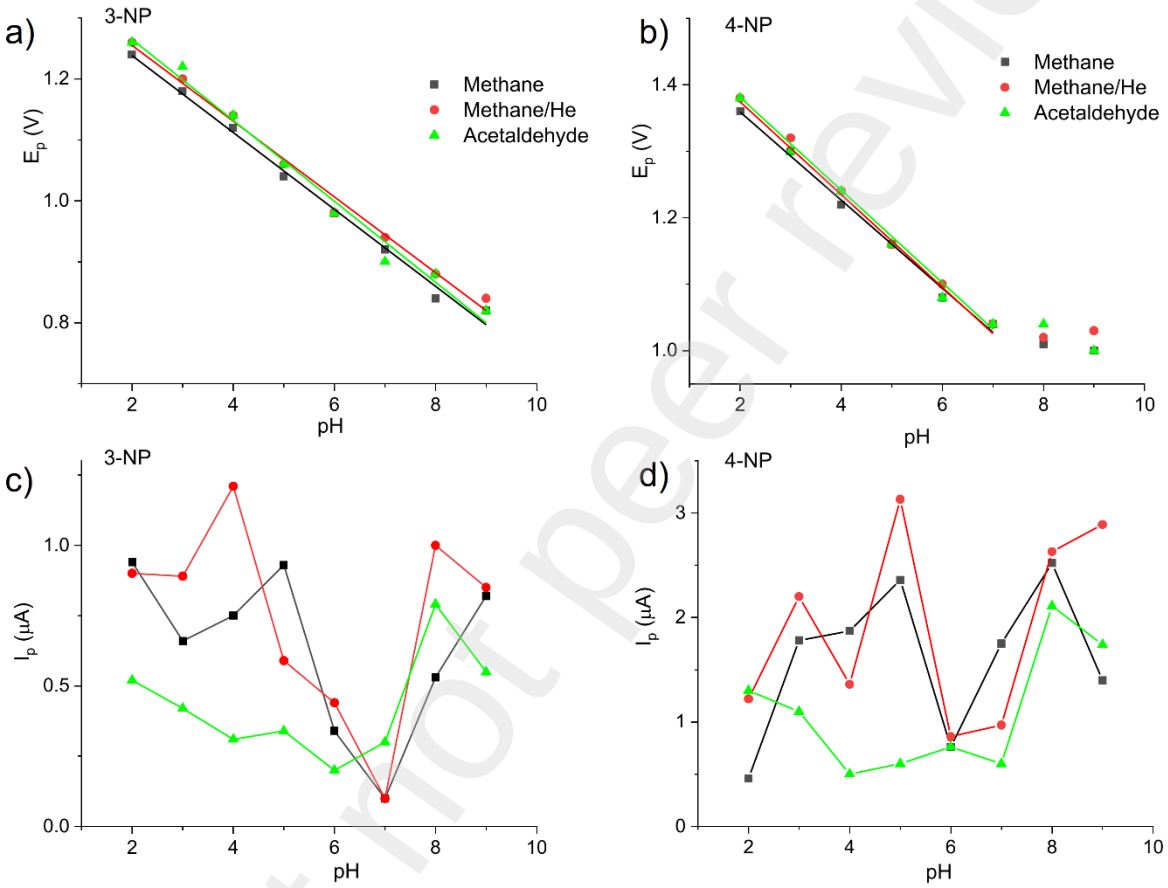

Figure 6: Dependence of peak potential and peak current on pH for oxidation of 1 mM 3-NP and 1 mM 4-NP on investigated graphene electrodes

The peak potential shifted to lower values with the increase in pH value. The values of slopes for the Ep vs. pH plot were in the range of 62 to 69 mV pH^{-1} for both 3-NP and 4-NP. These values are close to the value of 59 mV pH^{-1}, expected for the redox process with an equal number of protons and electrons exchanged. The peak potential of 4-NP oxidation was not pH dependent for pH values above 7, as can be expected since the pKa value of 4-NP is 7.2. The peak potential of 3-NP oxidation was pH dependent in the whole investigated pH range (the pKa value of 3-NP is 8.4).

The minimum current for 4-NP was obtained at pH 6 for Methane, while for 3-NP at pH 7. The currents obtained for the Acetaldehyde electrode were significantly lower than the currents obtained for the Methane and Methane/He electrodes in the pH range of 2-7. The currents obtained at pH 8 were comparable for all investigated electrodes. The dependence of peak current on pH value depended on two factors: the influence of pH on the surface groups of electrodes and the form of nitrophenols at given pH (protonated or deprotonated). The minimum current was probably obtained for pH values when the electrostatic repulsion between the electrode surface and nitrophenol was highest and the concentration of H^+ ions required proton-electron coupled reaction was lowest.

3.6 Electrochemical reduction of 4-NP and 3-NP

The cyclic voltammograms of reduction of 3-NP and 4-NP on the Methane electrode are presented in Figures 7a and 7b. Figures 7c and 7d represent the second cycle.

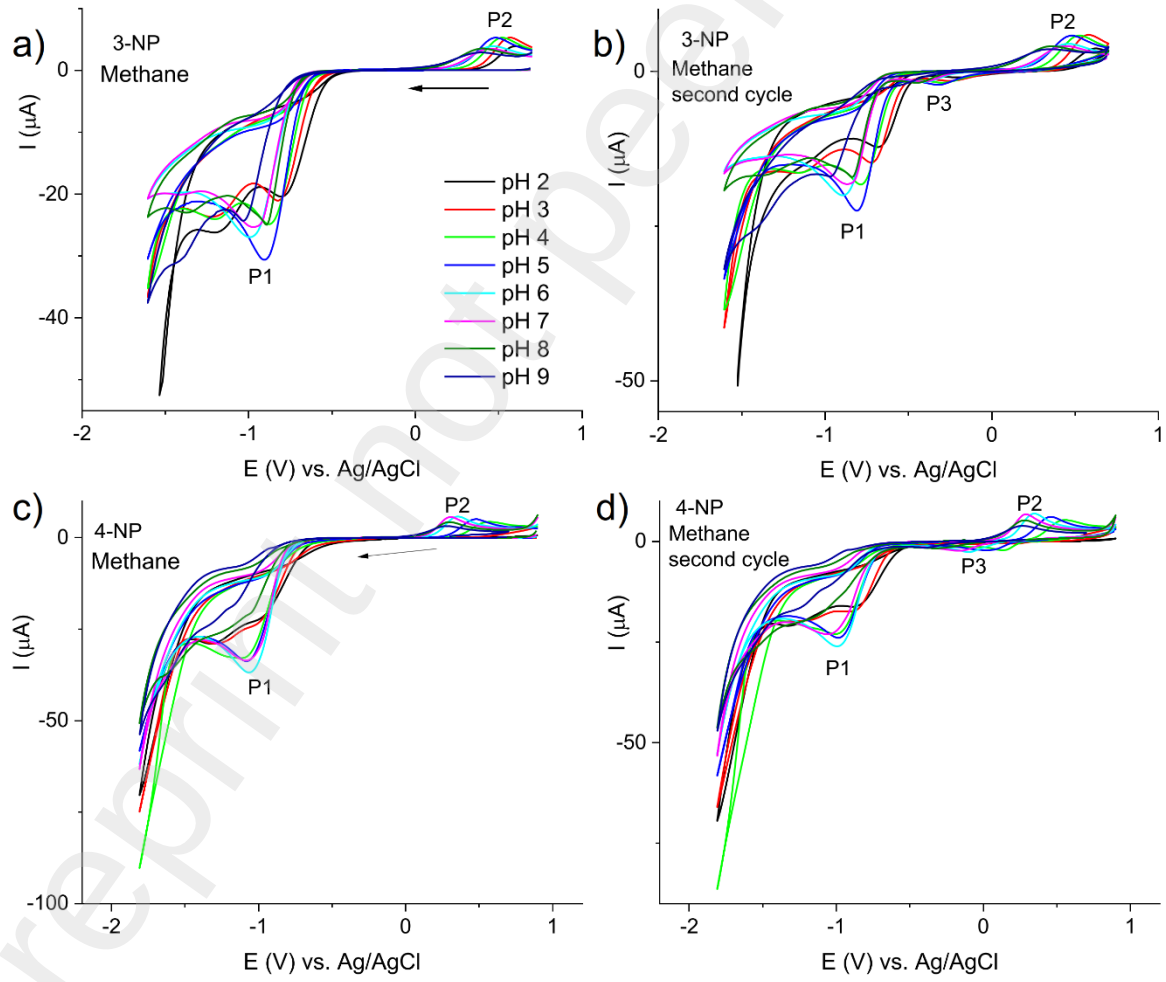

Figure 7: Cyclic voltammograms of electroreduction of a) 1 mM 3-NP and b) 1 mM 4-NP on Methane electrode recorded in the Britton-Robinson buffer at pH 5 at the scan rate of 100 mV s^{-1}; c) and d) second cycles recorded under the same conditions

The cyclic voltammograms of 3-NP and 4-NP electro-reduction are presented in Supplementary data as Figures S20 and S21. The scanning was performed toward negative potential as indicated with the arrow. In the negative going scan the cathodic peak due to the reduction of 3-nitrophenol is followed by the reduction peak of the oxygen functional group of graphene. The reduction peak of 4-NP was not clearly resolved at all pH values because it was shifted toward more negative values, overlapping with the reduction peak of the oxygen functional group of graphene. As opposed to the oxidation current, 3-NP reduction currents obtained for these three electrodes were not significantly different. The highest current of 3-NP reduction was obtained at pH 5 and 4-NP at pH 6 for all investigated electrodes.

In the forward-going scan, the anodic peak appeared due to the oxidation of the nitrophenol intermediate formed during a reduction in the negative scan. In the second cycle, another cathodic peak appears at a potential range of 0.2 to -0.2 for 4-NP and -0.1 to -0.4 for 3-NP, corresponding to the reduction of the intermediate. The peak current P1 decreased as a consequence of the electrode fouling by-products of nitrophenol electro-reduction. According to the literature data, these peaks can be ascribed to the following steps [37]:

P1: $-NO_2 + 4e^- + 4H^+ \rightarrow -NHOH + H_2O$ (4)

P2/P3: $-NHOH \Leftrightarrow -NO + 2H^+ + 2e^-$. (5)

The dependence of the peak potential of P3 peak for 3-NP and 4-NP on pH value is presented in Figure 8, for all investigated electrodes. The potential of the reaction depends on the pH according to the equation [29]:

$$E_p = -2.303\frac{mRT}{nF}pH \quad (6)$$

where m and n are the number of protons and electrons involved in the oxidation, respectively, R is the gas constant, T is the temperature, and F is the Faraday constant.

If the mechanism follows equations (4) and (5), the expected slope value is 59 mV pH^{-1}. The values of slopes for the Ep vs. pH plot were 48 mV pH^{-1} and 102 mV pH^{-1} for 3-NP and 4-NP, respectively.

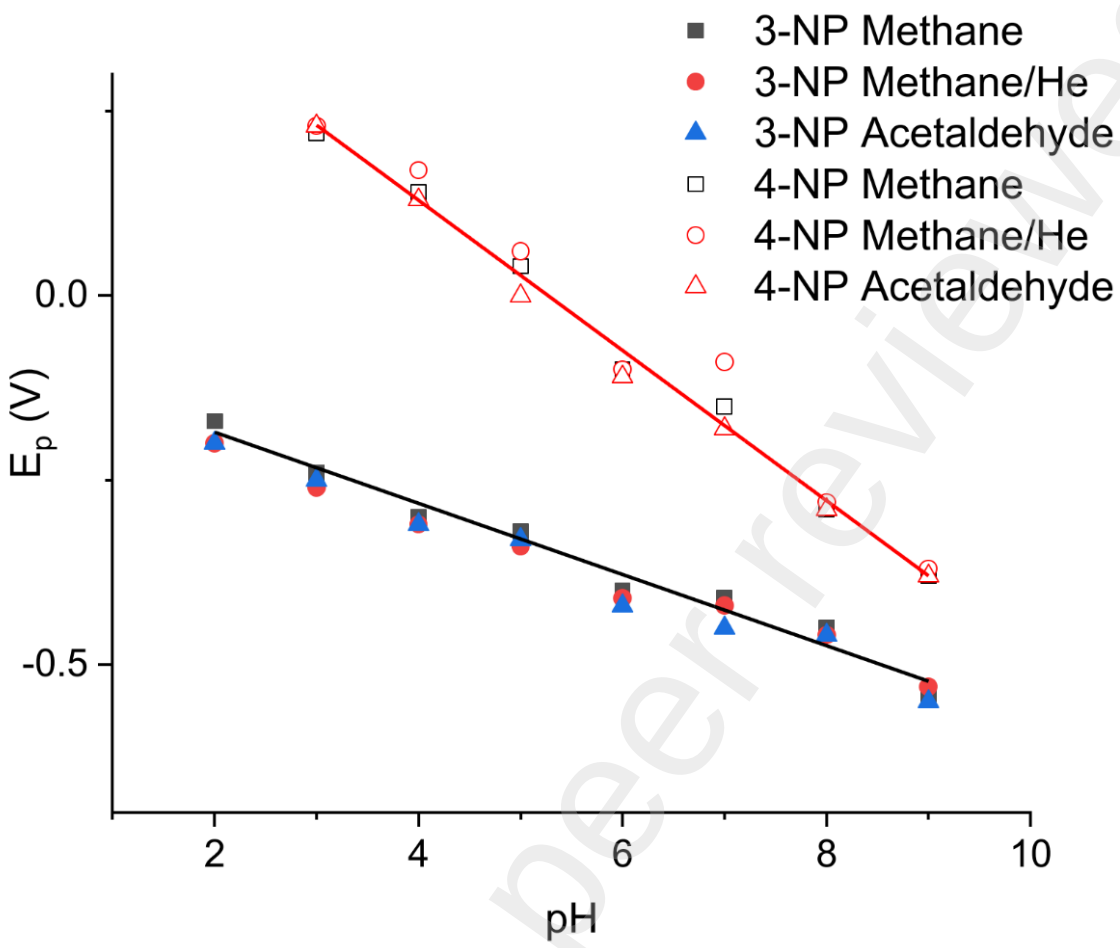

Figure 8: Dependence of peak potential P3 on pH for 3-NP and 4-NP on investigated graphene electrodes

The values obtained for 3-NP and 4-NP showed that oxidation of their intermediate followed different pathways. The mechanisms for the 3-NP intermediate followed the $1H^{+}2e^{-}$ pathway, while the 4-NP intermediate followed the $2H^{+}1e^{-}$ pathway. The reduction of nitrophenols occurs at the potential of reduction of oxygen-containing functionalities causing the formation of different intermediate species. The different response can be explained through the combination effects of different resonance structures and their interaction with the graphene surface groups. The difference of reactivity of aminophenol isomers with the graphene surface was reported by Gao et al [38]

The difference in peak potential for the P3 process for 3-NP and 4-NP was exploited for their simultaneous determination. The determination was performed by square wave voltammetry under optimized conditions. In order for the intermediate to be available for reduction, the electrode was polarized at a negative potential of -1.2 V for 30 s. The recording was performed

with the following parameters: amplitude 0.06 V, step 0.005 V and frequency 25 Hz. Square wave voltammograms obtained for the detection of equimolar concentrations of 3-NP and 4-NP in the concentration range of 10 µM to 1 mM are presented in Figure 9a, while the calibration plot is presented in Figure 9b.

The current response for 3-NP was linear in the concentration range from 10 to 1000 µM with the linear regression equation: I_p (µA) = -0.0819 + 0.0053 × $C_{3\text{-NP}}$ (µM); (R^2 = 0.9971). The current response for 4-NP was linear in the concentration range from 10 to 500 µM with the linear regression equation: I_p (µA) = 0.0596 + 0.0013 × $C_{4\text{-NP}}$ (µM) ; (R^2 = 0.9936).

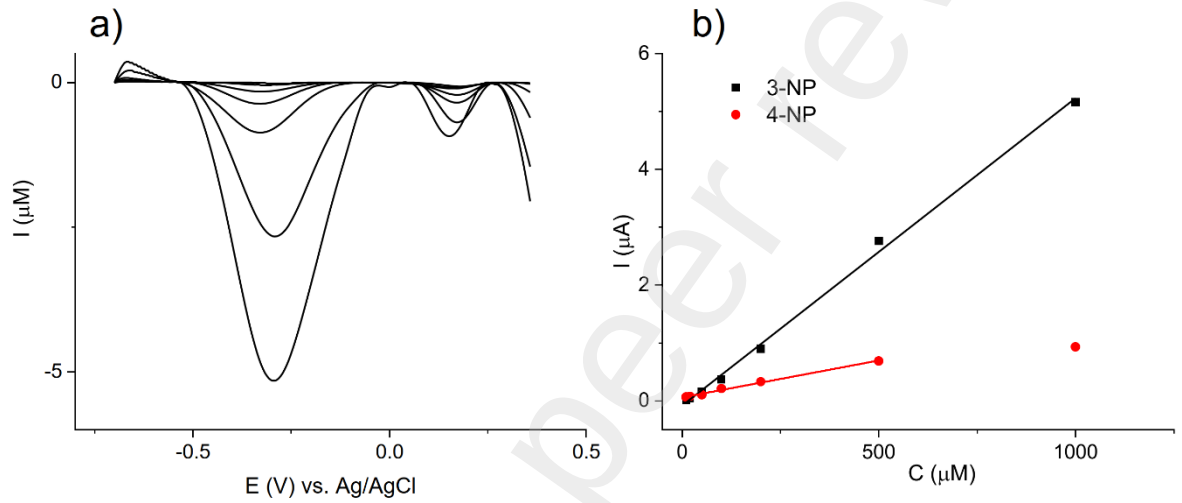

Figure 9: a) Square wave voltammograms recorded at pH 5 for the equimolar concentration of 3-NP and 4-NP in the concentration range 10 to 1000 µM; b) calibration plot

The comparison of the analytical performance of the Methane electrode for electrochemical sensing of 3-NP and 4-NP with that of other graphene-based electrodes reported in the literature is presented in Table 2.

Table 2: Comparison of the analytical performance at various graphene-based electrodes in the determination of 3-NP and 4-NP.

Electrode	Linear range (µM) 3-NP	Linear range (µM) 4-NP	Reference
RGO/GCE		50–800	[39]
NiO-NPs-α-CD-rGO-GCE		1 -10	[40]
PDPP–GO/GCE		0.5-163	[41]
ERGO/CTAB	0.5-100		[42]
GR/ABPE		0.02-100	[43]
GR-CS/GCE		0.1-140	[44]
SBCD-rGO/GCE	0.1-800	0.1-700	[45]
Methane derived graphene	10-1000	10-500	This work

The review of literature data shows that the obtained sensitivity and linear concentration range are somewhat below those obtained by other researchers using graphene. However, it should be pointed out, that graphene used for these measurements was not modified in any manner. Furthermore, there is very little literature data on the simultaneous detection of nitrophenol derivatives using graphene-based electrodes.

5. Conclusions

Herein, the electrochemical properties of the electrodes based on the graphene were presented and discussed. The graphene was obtained via continuous method in RF thermal plasma from various organic precursors. The materials exhibit nanoflake morphology and contain oxygen moieties, found with XPS. The present work showed that the electroactivity of synthesized graphene depended on the selected precursor. The electrochemical characterization showed that the electrode kinetics of $[Fe(CN)_6]^{4-/3-}$ and $[Ru(NH_3)_6]^{3+/2+}$ probe on graphene electrodes depended on the number of edge sites and the amount of oxygen. The highest activity for both redox probes was obtained for samples containing oxygen in the amount of 3-4 atomic % of surface composition. Additionally, the type of carbon-oxygenated species also influenced the response of investigated graphene electrodes. Species C=O and C-O-C had a positive effect on the charge transfer kinetics for both redox probes, while C–O–C in ester, OH in the carboxyl and C-OH had a negative effect. The best performance for nitrophenol detection was obtained for graphene obtained from methane, i.e. the sample with the highest content of edge sites and the adequate surface composition. However, another analyte might require graphene with different properties. The choice of the right precursor might deliver the graphene with the right set of properties for certain analytes.

Acknowledgements

The electrochemical characterization of the graphene materials was financially supported by the Ministry of Science, Technological Development and Innovation of the Republic of Serbia (Grant No. 451-03-47/2023-01/200026).

The postdoctoral internship of dr. Maciej Fronczak at the University of Belgrade, Institute of Chemistry, Technology and Metallurgy, Department for Catalysis and Chemical Engineering was financially supported by Polish National Agency for Academic Exchange (NAWA) (contract no. PPN/BIL/2020/1/00016) within the exchange program for students and scientists as part of bilateral cooperation.

The graphene synthesis was performed during postdoctoral internship of dr. Maciej Fronczak at Institute of Materials and Environmental Chemistry, Research Centre for Natural Sciences, Budapest, Hungary within the Bekker Program by Polish National Agency for Academic Exchange (NAWA) (contract no. PPN/BEK/2020/1/00013).

The authors also acknowledge the support given by the Hungarian National Research Development and Innovation Office for the funding of project No. VEKOP-2.3.2-16-2017-00013 supported by the European Union and the State of Hungary, co-financed by the European Regional Development Fund.

The authors thank Anna Maria Keszler, Miklós Mohai and Bálint Jezsó from the Institute of Materials and Environmental Chemistry, Research Centre for Natural Sciences for their support during the synthesis and characterization of graphene materials.

Bibliography

[1] Q. Zhou, H. Yao, Recent development of carbon electrode materials for electrochemical supercapacitors, Energy Reports. 8 (2022) 656–661. https://doi.org/10.1016/j.egyr.2022.09.167.

[2] F. Rehman, F.H. Memon, A. Ali, S.M. Khan, F. Soomro, M. Iqbal, K.H. Thebo, Recent progress on fabrication methods of graphene-based membranes for water purification, gas separation, and energy sustainability, Rev. Inorg. Chem. 43 (2023) 13–31. https://doi.org/10.1515/revic-2022-0001.

[3] R.L. McCreery, Advanced Carbon Electrode Materials for Molecular Electrochemistry, Chem. Rev. 108 (2008) 2646–2687. https://doi.org/10.1021/cr068076m.

[4] A.N. Patel, M.G. Collignon, M.A. O'Connell, W.O.Y. Hung, K. McKelvey, J. V. Macpherson, P.R. Unwin, A New View of Electrochemistry at Highly Oriented Pyrolytic Graphite, J. Am. Chem. Soc. 134 (2012) 20117–20130. https://doi.org/10.1021/ja308615h.

[5] K.D. Patel, R.K. Singh, H.-W. Kim, Carbon-based nanomaterials as an emerging platform for theranostics, Mater. Horizons. 6 (2019) 434–469. https://doi.org/10.1039/C8MH00966J.

[6] K.S. Novoselov, A.K. Geim, S. V. Morozov, D. Jiang, Y. Zhang, S. V. Dubonos, I. V. Grigorieva, A.A. Firsov, Electric Field Effect in Atomically Thin Carbon Films, Science (80-.). 306 (2004) 666–669. https://doi.org/10.1126/science.1102896.

[7] R. Raccichini, A. Varzi, S. Passerini, B. Scrosati, The role of graphene for electrochemical energy storage, Nat. Mater. 14 (2015) 271–279. https://doi.org/10.1038/nmat4170.

[8] D. Higgins, P. Zamani, A. Yu, Z. Chen, The application of graphene and its composites in oxygen reduction electrocatalysis: a perspective and review of recent progress, Energy Environ. Sci. 9 (2016) 357–390. https://doi.org/10.1039/C5EE02474A.

[9] M. Pumera, A. Ambrosi, A. Bonanni, E.L.K. Chng, H.L. Poh, Graphene for electrochemical sensing and biosensing, TrAC Trends Anal. Chem. 29 (2010) 954–965. https://doi.org/10.1016/j.trac.2010.05.011.

[10] A. Ambrosi, C.K. Chua, A. Bonanni, M. Pumera, Electrochemistry of Graphene and Related Materials, Chem. Rev. 114 (2014) 7150–7188.

https://doi.org/10.1021/cr500023c.

[11] D.A.C. Brownson, L.J. Munro, D.K. Kampouris, C.E. Banks, Electrochemistry of graphene: not such a beneficial electrode material?, RSC Adv. 1 (2011) 978. https://doi.org/10.1039/c1ra00393c.

[12] T.J. Davies, M.E. Hyde, R.G. Compton, Nanotrench Arrays Reveal Insight into Graphite Electrochemistry, Angew. Chemie Int. Ed. 44 (2005) 5121–5126. https://doi.org/10.1002/anie.200462750.

[13] T.J. Davies, R.R. Moore, C.E. Banks, R.G. Compton, The cyclic voltammetric response of electrochemically heterogeneous surfaces, J. Electroanal. Chem. 574 (2004) 123–152. https://doi.org/10.1016/j.jelechem.2004.07.031.

[14] S.C.S. Lai, A.N. Patel, K. McKelvey, P.R. Unwin, Definitive Evidence for Fast Electron Transfer at Pristine Basal Plane Graphite from High-Resolution Electrochemical Imaging, Angew. Chemie Int. Ed. 51 (2012) 5405–5408. https://doi.org/10.1002/anie.201200564.

[15] M. Jindra, M. Velický, M. Bouša, G. Abbas, M. Kalbáč, O. Frank, Localized Spectroelectrochemical Identification of Basal Plane and Defect-Related Charge-Transfer Processes in Graphene, J. Phys. Chem. Lett. 13 (2022) 642–648. https://doi.org/10.1021/acs.jpclett.1c03466.

[16] C.X. Lim, H.Y. Hoh, P.K. Ang, K.P. Loh, Direct Voltammetric Detection of DNA and pH Sensing on Epitaxial Graphene: An Insight into the Role of Oxygenated Defects, Anal. Chem. 82 (2010) 7387–7393. https://doi.org/10.1021/ac101519v.

[17] Q. Li, C. Batchelor-McAuley, R.G. Compton, Electrochemical Oxidation of Guanine: Electrode Reaction Mechanism and Tailoring Carbon Electrode Surfaces To Switch between Adsorptive and Diffusional Responses, J. Phys. Chem. B. 114 (2010) 7423–7428. https://doi.org/10.1021/jp1021196.

[18] M. Pumera, R. Scipioni, H. Iwai, T. Ohno, Y. Miyahara, M. Boero, A Mechanism of Adsorption of β-Nicotinamide Adenine Dinucleotide on Graphene Sheets: Experiment and Theory, Chem. - A Eur. J. 15 (2009) 10851–10856. https://doi.org/10.1002/chem.200900399.

[19] D.A.C. Brownson, D.K. Kampouris, C.E. Banks, Graphene electrochemistry: fundamental concepts through to prominent applications, Chem. Soc. Rev. 41 (2012)

6944. https://doi.org/10.1039/c2cs35105f.

[20] N.S. Suhaimin, M.F.R. Hanifah, M. Azhar, J. Jaafar, M. Aziz, A.F. Ismail, M.H.D. Othman, M.A. Rahman, F. Aziz, N. Yusof, R. Mohamud, The evolution of oxygen-functional groups of graphene oxide as a function of oxidation degree, Mater. Chem. Phys. 278 (2022) 125629. https://doi.org/10.1016/j.matchemphys.2021.125629.

[21] I. Ferrari, A. Motta, R. Zanoni, F.A. Scaramuzzo, F. Amato, E.A. Dalchiele, A.G. Marrani, Understanding the nature of graphene oxide functional groups by modulation of the electrochemical reduction: A combined experimental and theoretical approach, Carbon N. Y. 203 (2023) 29–38. https://doi.org/10.1016/j.carbon.2022.11.052.

[22] K.A. Madurani, S. Suprapto, N.I. Machrita, S.L. Bahar, W. Illiya, F. Kurniawan, Progress in Graphene Synthesis and its Application: History, Challenge and the Future Outlook for Research and Industry, ECS J. Solid State Sci. Technol. 9 (2020) 093013. https://doi.org/10.1149/2162-8777/abbb6f.

[23] M. Fronczak, A.M. Keszler, M. Mohai, B. Jezsó, A. Farkas, Z. Károly, Facile and continuous synthesis of graphene nanoflakes in RF thermal plasma, Carbon N. Y. (2022). https://doi.org/10.1016/j.carbon.2022.03.008.

[24] J. Xu, Y. Wang, S. Hu, Nanocomposites of graphene and graphene oxides: Synthesis, molecular functionalization and application in electrochemical sensors and biosensors. A review, Microchim. Acta. 184 (2017) 1–44. https://doi.org/10.1007/s00604-016-2007-0.

[25] M. Coroş, S. Pruneanu, R.-I. Stefan-van Staden, Review—Recent Progress in the Graphene-Based Electrochemical Sensors and Biosensors, J. Electrochem. Soc. 167 (2020) 037528. https://doi.org/10.1149/2.0282003JES.

[26] L. Wang, Z. Sofer, M. Pumera, Will Any Crap We Put into Graphene Increase Its Electrocatalytic Effect?, ACS Nano. 14 (2020) 21–25. https://doi.org/10.1021/acsnano.9b00184.

[27] M. Fronczak, P. Fazekas, Z. Károly, B. Hamankiewicz, M. Bystrzejewski, Continuous and catalyst free synthesis of graphene sheets in thermal plasma jet, Chem. Eng. J. 322 (2017) 385–396. https://doi.org/10.1016/j.cej.2017.04.051.

[28] W.T. Yap, L.M. Doane, Determination of diffusion coefficients by chronoamperometry with unshielded planar stationary electrodes, Anal. Chem. 54 (1982) 1437–1439.

https://doi.org/10.1021/ac00245a041.

[29] A.J. Bard, L.R. Faulkner, Electrochemical Methods: Fundamentals and Applications, 2nd Edition, Wiley, 2000.

[30] R.S. Nicholson, Theory and Application of Cyclic Voltammetry for Measurement of Electrode Reaction Kinetics., Anal. Chem. 37 (1965) 1351–1355. https://doi.org/10.1021/ac60230a016.

[31] I. Lavagnini, R. Antiochia, F. Magno, An Extended Method for the Practical Evaluation of the Standard Rate Constant from Cyclic Voltammetric Data, Electroanalysis. 16 (2004) 505–506. https://doi.org/10.1002/elan.200302851.

[32] A.J. Slate, D.A.C. Brownson, A.S. Abo Dena, G.C. Smith, K.A. Whitehead, C.E. Banks, Exploring the electrochemical performance of graphite and graphene paste electrodes composed of varying lateral flake sizes, Phys. Chem. Chem. Phys. 20 (2018) 20010–20022. https://doi.org/10.1039/C8CP02196A.

[33] D.A.C. Brownson, S.A. Varey, F. Hussain, S.J. Haigh, C.E. Banks, Electrochemical properties of CVD grown pristine graphene: monolayer- vs. quasi-graphene, Nanoscale. 6 (2014) 1607–1621. https://doi.org/10.1039/C3NR05643K.

[34] R.M. Wightman, M.R. Deakin, P.M. Kovach, W.G. Kuhr, K.J. Stutts, Methods to Improve Electrochemical Reversibility at Carbon Electrodes, J. Electrochem. Soc. 131 (1984) 1578–1583. https://doi.org/10.1149/1.2115913.

[35] A.Y.S. Eng, A. Ambrosi, C.K. Chua, F. Šaněk, Z. Sofer, M. Pumera, Unusual Inherent Electrochemistry of Graphene Oxides Prepared Using Permanganate Oxidants, Chem. - A Eur. J. 19 (2013) 12673–12683. https://doi.org/10.1002/chem.201301889.

[36] A.G. Marrani, A. Motta, R. Schrebler, R. Zanoni, E.A. Dalchiele, Insights from experiment and theory into the electrochemical reduction mechanism of graphene oxide, Electrochim. Acta. 304 (2019) 231–238. https://doi.org/10.1016/j.electacta.2019.02.108.

[37] Q. Shi, M. Chen, G. Diao, Electrocatalytical reduction of m-nitrophenol on reduced graphene oxide modified glassy carbon electrode, Electrochim. Acta. 114 (2013) 693–699. https://doi.org/10.1016/j.electacta.2013.10.108.

[38] M. Salman, X. Chu, T. Huang, S. Cai, Q. Yang, X. Dong, K. Gopalsamy, C. Gao, Functionalization of wet-spun graphene films using aminophenol molecules for high performance supercapacitors, Mater. Chem. Front. 2 (2018) 2313–2319.

https://doi.org/10.1039/C8QM00260F.

[39] P. Wiench, B. Grzyb, Z. González, R. Menéndez, B. Handke, G. Gryglewicz, pH robust electrochemical detection of 4-nitrophenol on a reduced graphene oxide modified glassy carbon electrode, J. Electroanal. Chem. 787 (2017) 80–87. https://doi.org/10.1016/j.jelechem.2017.01.040.

[40] U. Solaem Akond, K. Barman, A. Mahanta, S. Jasimuddin, Electrochemical Sensor for Detection of p-Nitrophenol Based on Nickel Oxide Nanoparticles/α-Cyclodextrin Functionalized Reduced Graphene Oxide, Electroanalysis. 33 (2021) 900–908. https://doi.org/10.1002/elan.202060450.

[41] L. Jia, J. Hao, S. Wang, L. Yang, K. Liu, Sensitive detection of 4-nitrophenol based on pyridine diketopyrrolopyrrole-functionalized graphene oxide direct electrochemical sensor, RSC Adv. 13 (2023) 2392–2401. https://doi.org/10.1039/D2RA07239D.

[42] N. Muhammad, J. Abdullah, Y. Sulaiman, L.H. Ngee, Electrochemical Determination of 3-Nitrophenol with a Reduced Graphene Oxide Modified Screen Printed Carbon Electrode, Sens. Lett. 15 (2017) 187–195. https://doi.org/10.1166/sl.2017.3785.

[43] Q. He, Y. Tian, Y. Wu, J. Liu, G. Li, P. Deng, D. Chen, Facile and Ultrasensitive Determination of 4-Nitrophenol Based on Acetylene Black Paste and Graphene Hybrid Electrode, Nanomaterials. 9 (2019) 429. https://doi.org/10.3390/nano9030429.

[44] J. Tang, L. Zhang, G. Han, Y. Liu, W. Tang, Graphene-Chitosan Composite Modified Electrode for Simultaneous Detection of Nitrophenol Isomers, J. Electrochem. Soc. 162 (2015) B269–B274. https://doi.org/10.1149/2.0811510jes.

[45] L. Cong, Z. Ding, T. Lan, M. Guo, F. Yan, J. Zhao, Simultaneous determination of nitrophenol isomers based on reduced graphene oxide modified with sulfobutylether-β-cyclodextrin, Carbohydr. Polym. 271 (2021) 118446. https://doi.org/10.1016/j.carbpol.2021.118446.